Electronic Supplementary Material (ESI) for Nanoscale.
This journal is © The Royal Society of Chemistry 2021

Electronic Supplementary Information (ESI)

Engineering the oxygen vacancies of rocksalt type high-entropy oxides for enhanced electrocatalysis

Yaohang Gu[1], Ateer Bao[1], Xuanyu Wang[1], Yizhen Chen[5], Liang Dong[3,4], Xin Liu[1,3], Haijun Pan[3,], Ying Li[6], and Xiwei Qi[2,]**

[1]School of Materials Science and Engineering, Northeastern University, Shenyang 110189, China

[2]College of Metallurgy and Energy, North China of Science and Technology, Tangshan 063210, China

[3]School of Resources and Materials, Northeastern University at Qinhuangdao, Qinhuangdao 066004, China

[4]Key Laboratory of Dielectric and Electrolyte Functional Material Hebei Province, Northeastern University at Qinhuangdao, Qinhuangdao 066004, China

[5]Hefei National Laboratory for Physical Sciences at the Microscale, University of Science and Technology of China, Hefei, Anhui 230026, China

[6]School of science, Inner Mongolia University of Science and Technology, Baotou 014010, China

*Corresponding authors E-mail address: panhaijun@neuq.edu.cn; qxw@mail.neuq.edu.cn

This part includes:

References (Page S28)

1. Experimental

1.1 Synthesis of LTM series sample

All of the LTM series compounds were synthesized by a modified solid-state method. $LiNO_3$•$6H_2O$ (Aladdin, 99%), $Fe(NO_3)_3$•$9H_2O$ (Sinopharm, 98.5%), $Co(NO_3)_2$•$6H_2O$ (Aladdin, 99%), $Ni(NO_3)_2$•H_2O (Aladdin, 98%), $Cu(NO_3)_2$•H_2O (Sinopharm, 99%) and $Zn(NO_3)_2$•H_2O (Aladdin, 99%) were used as precursors for synthesizing the HEOs. For LTM16.7, 10mmol of each precursor was stoichiometrically dissolved in 50 mL deionized water under vigorous stirring for 2h. Cotton purchased from local pharmacy was soaked in the above solution with 5h soaking treatment. The cotton we used is to absorb the corresponding metal nitrate to prevent the aggregation during the calcination process. For the purpose of eliminating the cotton precursor with a mild process, the heat treatment under 400℃ is required. After the damp cotton was totally dried, all of the cotton was transferred to a box furnace and heated in air to a temperature of 400℃ with the heating rate of 2℃ per minute. After cooling to room temperature, the resulting brown powder was grounded and returned to the furnace. Then it was calcined at 1150℃ which was maintained for 2h. Finally, the final obtained product was hand-grounded and sieved with 200 mesh. LTM0 and LTM12 could be obtained through tuning the molar ratio of Li precursors while keeping other precursors unchanged. The elemental alternation experiment was proceeded with the same method except that only one metal element was removed for each sample. For Mg-substituted sample, all the samples was prepared with the same process but replaced with the equimolar Mg. The NaFeCoNiCuZnO and KFeCoNiCuZnO was prepared with the same method which replaced $NaNO_3$ and KNO_3 with the same mole with $LiNO_3$. FeCoNiO low entropy oxides was prepared with equimolar Fe, Co, and Ni source by the same process as well.

1.2 Characterization

Phase identification was performed by Smartlab X-ray diffractometer (Rigaku, Japan) using Cu Kα radiation (λ=1.5406 Å) from 20° to 90° in the 2θ range. Rietveld refinement was operated using JANA 2006 program. The valences of surface atoms were measured by Escalab 250Xi X-ray photoelectron spectroscope (Thermo Fisher Scientific, USA) with Al Kα (hν=1486.6 eV), the attained data was fitted by the "XPSPEAK41" software. The high-resolution core levels and the

valence band position spectra were performed at constant pass energy of 50 eV and 0.05 eV per step. SEM images were collected using a Supra-55 scanning electron microscope (Zeiss, Germany). STEM/EDS/selected area electron diffraction characterization were carried out by a Tecnai G2 F20 (FEI, American) and JEM-ARM200F (JEOL, Japan). The electron spin resonance (ESR) spectroscopy was conducted using Bruker A300 system (Germany). The electrical transport property was measured on a TH2839 precision impedance analyzer with temperature control system (China). And Hall coefficient were obtained by HMS-7000 electronics transport measurement system at room temperature (Ecopia, Korea). ^{57}Fe Mössbauer spectra was collected in the laboratory using MS500 (Wissel, Germany). The soft X-ray absorption find structure spectra (XAS) Co K-edge were collected at BL14W1 beamline of Shanghai Synchrotron Radiation Facility (SSRF). The data were collected in fluorescence mode using a Lytle detector while the corresponding reference sample were collected in transmission mode. The sample were grinded and uniformly daubed on the special adhesive tape.

1.3 Electrochemical Measurements

The overall water splitting performance was evaluated with a three-electrode system in 1 M aqueous KOH solution on a CHI-760E electrochemical workstation (Chenhua, China). Ag/AgCl (KCl, 3M) and carbon were used as reference and counter electrode, respectively. To prepare working electrode, 2 mg of the as-prepared catalysts, 0.5 mg of conductive carbon (Ketjen black EC300J), and 10 μL of 5 wt.% Nafion solution was dispersed in 495 μL water and 495 μL ethanol with the ultrasonication treatment for at least for 60 min to form a homogenous ink. Then the catalyst ink was cast onto carbon fiber paper (1cm×1cm, thickness 0.19 mm) to achieve a loading mass of 2 mg cm^{-2} for the geometric surface area of catalyst on the carbon fiber paper is 1 cm^2. After treated with an IR lamp, the as-prepared working electrode can be used for the electrochemical characterization. Before electrochemical test, the LSV polarization curve was obtained at a scan rate of 2 mV s^{-1} after 20 sweeps of cyclic voltammetry (CV) cycling. The LSV curves were corrected for IR-drop compensation using ohmic resistance by the electrochemical impedance spectroscopy (EIS), which the EIS was carried out under the same configuration by applying an AC voltage of 5 mV amplitude at the overpotential of 280 mV for HER and 310 mV for OER. The EDLC measurements were operated by the CV methods with 2 cycles between 0 and 0.1 versus RHE at the scanning rates of 5, 10, 15, 20, and 25 mV s^{-1}. The slope of current density at 0.05 V versus RHE and the scanning rates plots were used to determine the EDLC value.

The stability measurements were collected under a at a constant potential for obtaining the *i-t* curves. For ORR tests, a rotating disk electrode (RDE) made of glassy carbon (GC, 0.126 cm^2) was used as working electrode, which was prepared by a controlled drop-casting method with 10 μL of catalyst ink onto the polished surface of glassy carbon. The LSV curves were operated by using RDE at different rotation speeds (100, 400, 900, 1600, 2500, 3600 rpm) in O_2-saturated 0.1 M KOH at the scan rate of 5 mV s^{-1}.

1.4 DFT calculation

LiFeCoNiCuZnO in periodic rocksalt structure is generated by special quasi-random structures (SQS) in the alloy automated toolkit (ATAT), as shown in Fig. S17. The atomic distributions were selected so that the cluster association is as close as possible to the expected value in the random atomic arrangement under a given structure size. The (011) facet was chosen as the exposed surface according to our TEM results. All calculations were carried out by using the DFT framework implemented in the Vienna ab initio simulation package (VASP). The pseudopotential suggesting electron-ion interactions was described by the projector augmented wave (PAW) method. The generalized gradient approximation of Perdew, Burke and Ernzerhof was used as the exchange-correlation function, and a plane-wave basis set with a cutoff of 500 eV was utilized. Structural relaxation was reached based on a convergence of total energy within 10^{-4} eV and a force on each atom of <0.01 eV $Å^{-1}$. The Brilluoin zone was sampled with 11×11×11 mesh of special k points for bulk and 3×3×1 for surface reaction calculations.

Supporting evidences

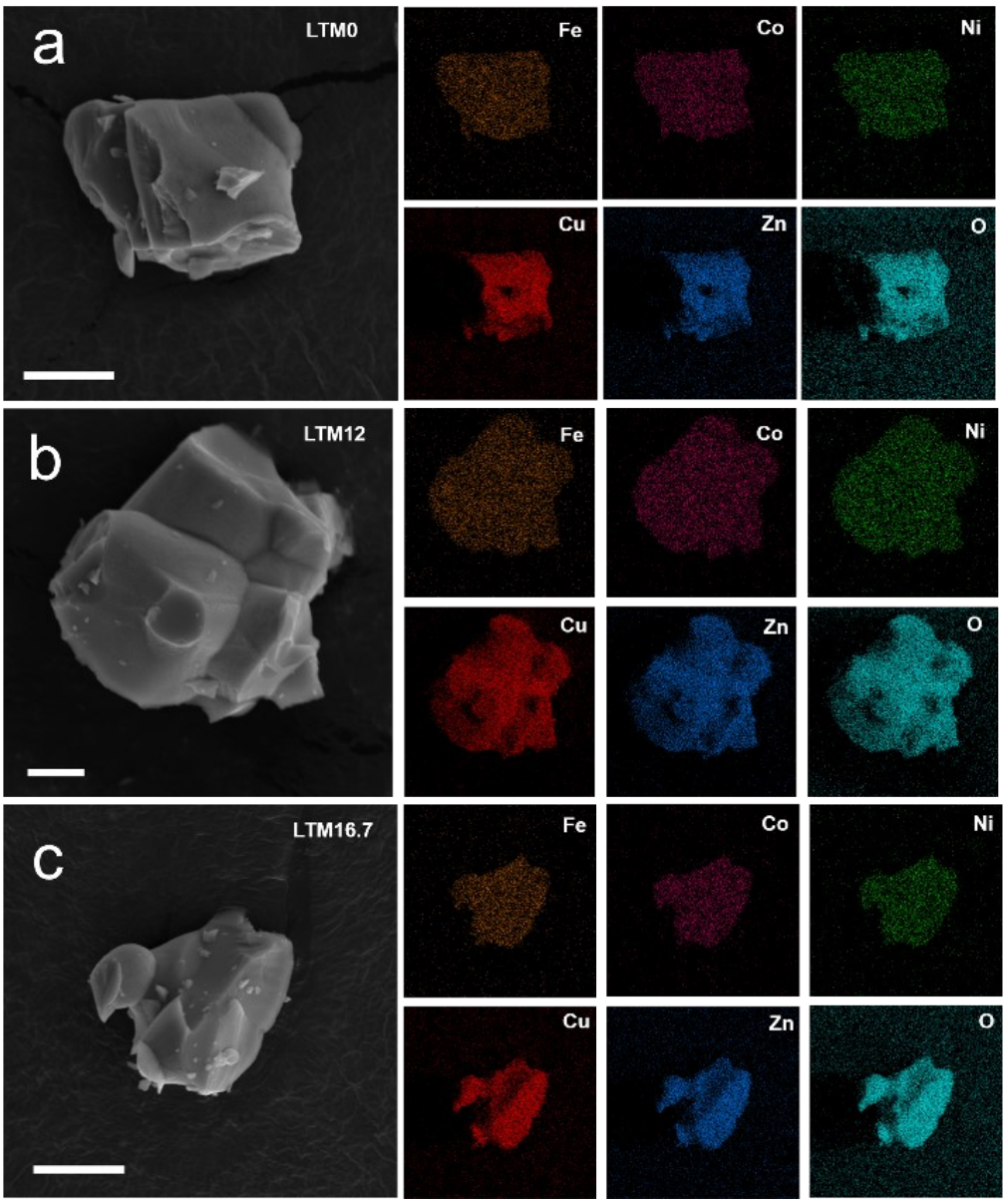

Fig. S1. SEM images and corresponding elemental maps of (a) LTM0; (b) LTM12; (c) LTM16.7. Scale bars indicates 5 μm.

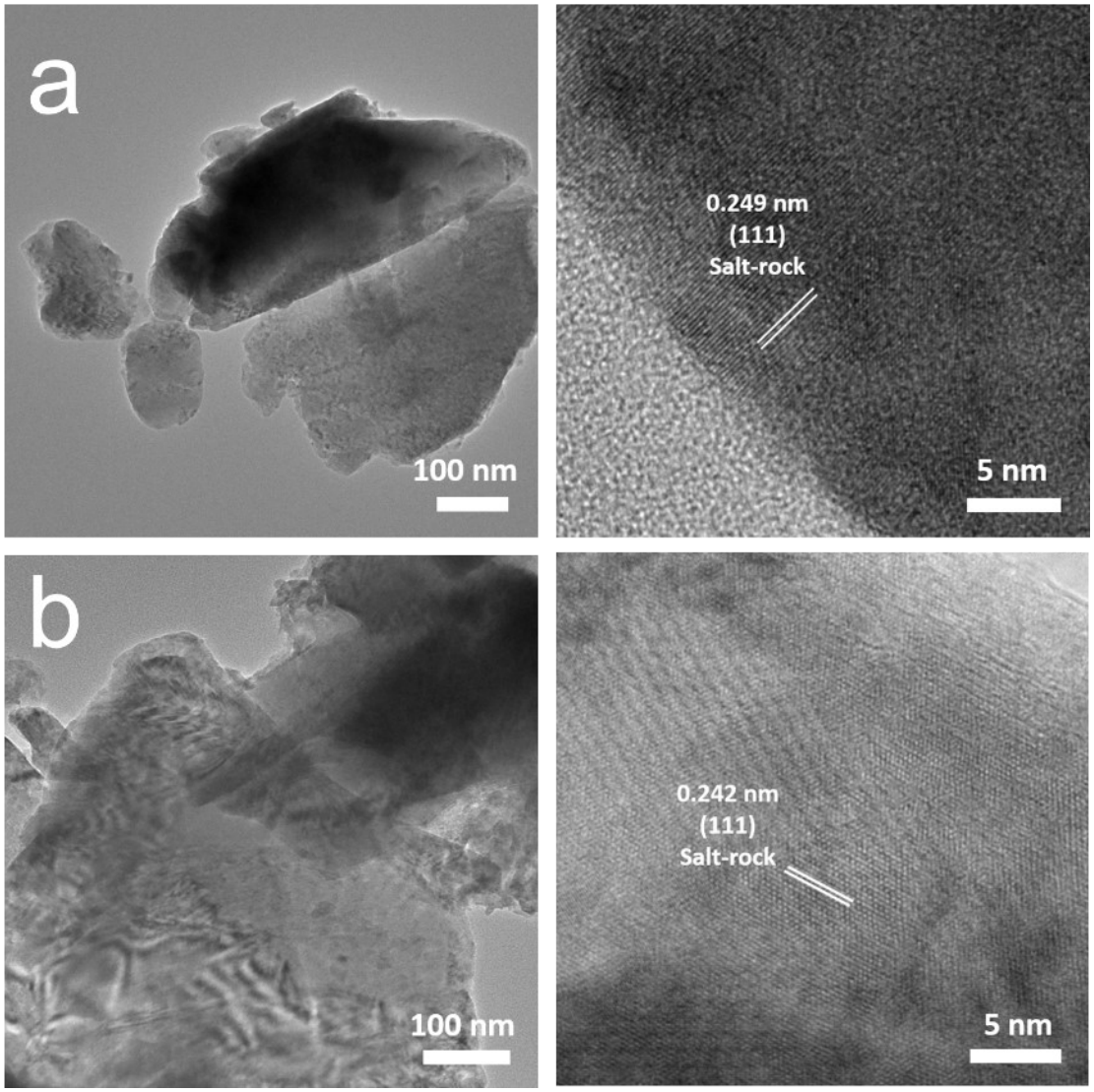

Fig. S2. TEM and HRTEM images of (a) LTM0 and (b) LTM12.

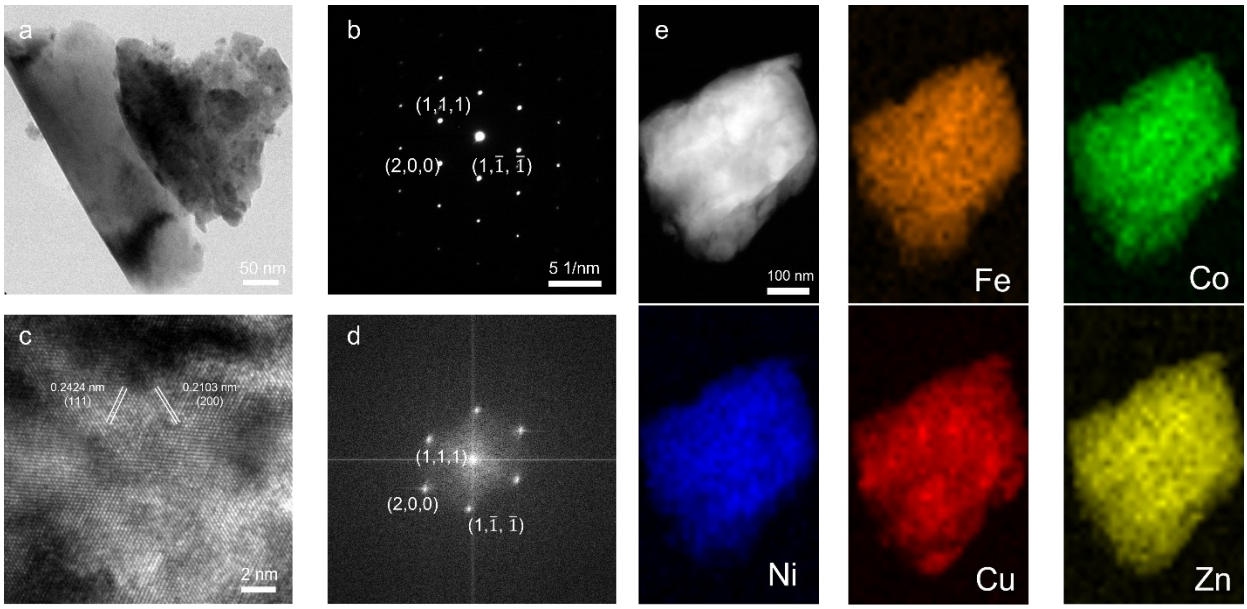

Fig. S3. (a) TEM image; (b) SAED pattern; (c) HRTEM; (d) Corresponding FFT results in c; and (e) STEM-EDS mapping of elemental distribution of as-prepared LTM16.7 sample. Both the SAED pattern and FFT results show the single crystalline structure, and the indexed (2,0,0) and (1,1,1) facets suggest that (0,-1,1) facet is mainly exposed.

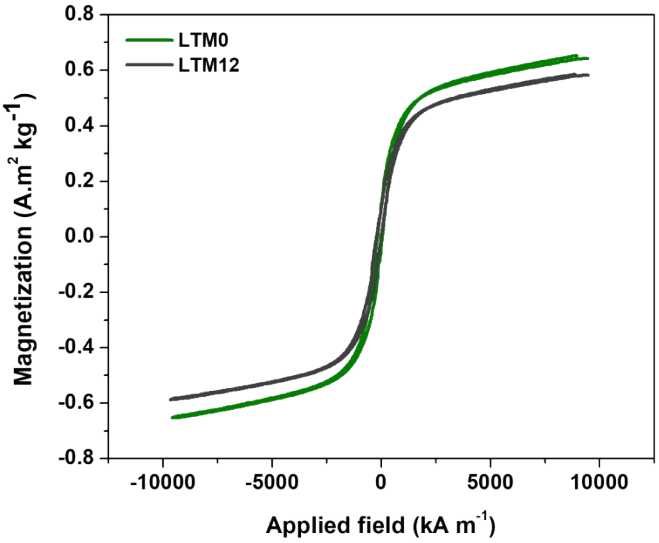

Fig. S4. Magnetization measurements on LTM0 and LTM12. For the LTM16.7, the disappearance of magnetic indicates that the variations of electronic structure at the 3d orbitals.

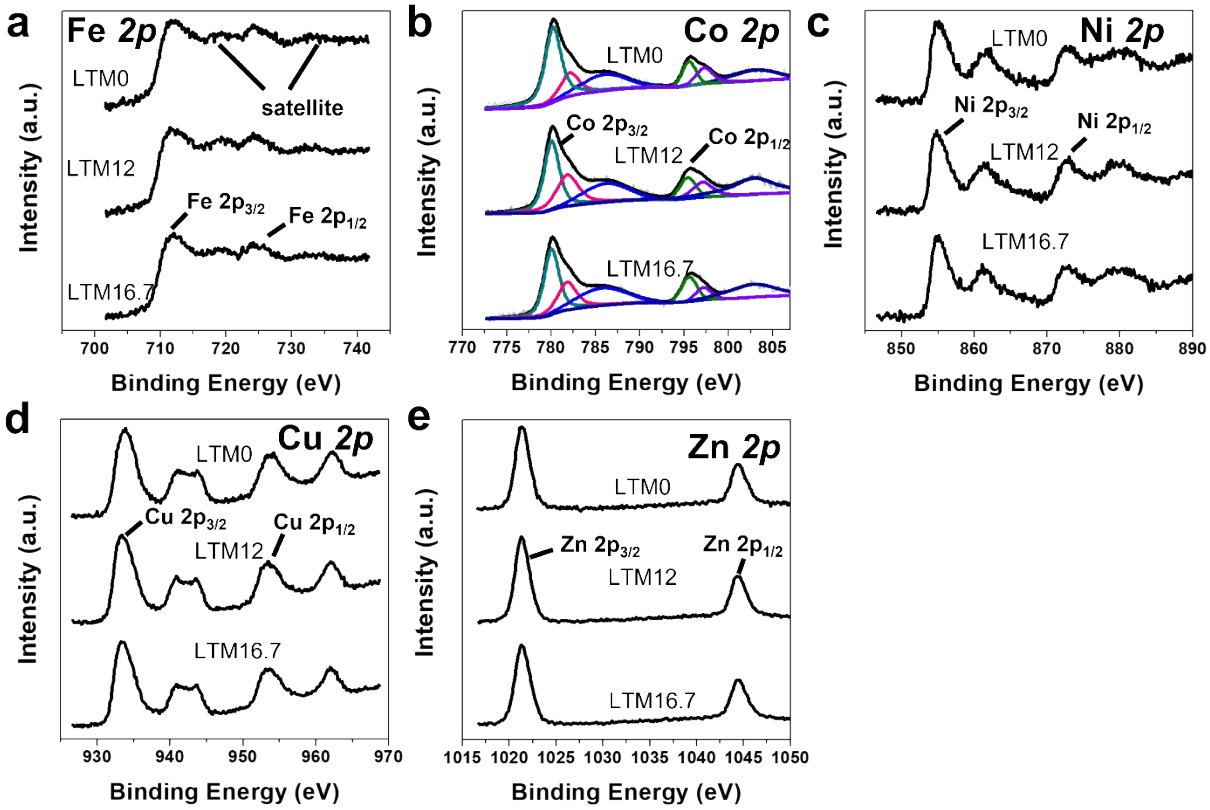

Fig. S5. XPS spectra of (a) Fe 2p; (b) Co 2p; (c) Ni 2p; (d) Cu 2p; (e) Zn 2p. XPS spectra of Fe 2p signal shows apparent shifts towards lower binding energy with increasement of Li content.

Table S1. Summary of Mössbauer spectrum fitting results.

Sample	IS	QS	W
LTM0	0.321	0.719	0.413
LTM12	0.362	0.556	0.417
LTM16.7	0.375	0.515	0.433

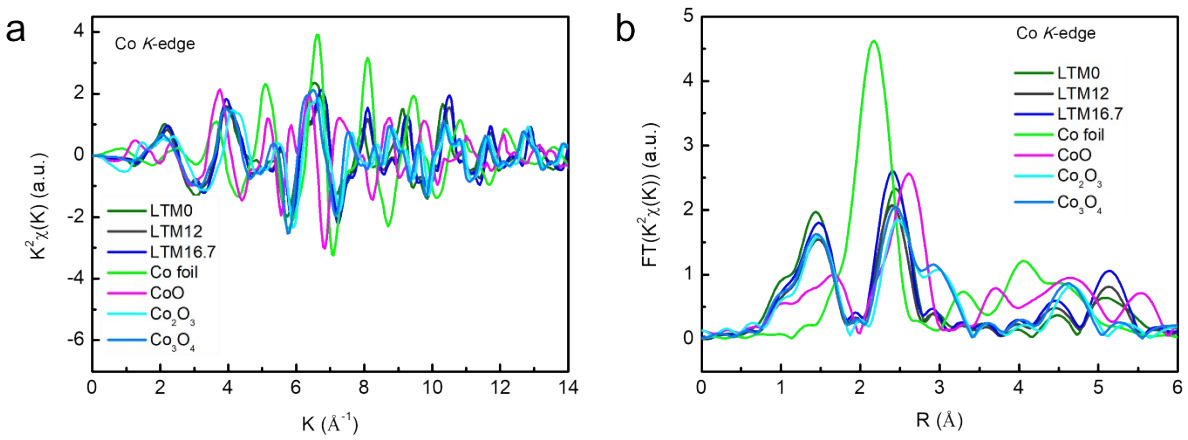

Fig. S6. (a) Co *K*-edge EXAFS data and (b) the corresponding k^3-weighted Fourier-transformed data.

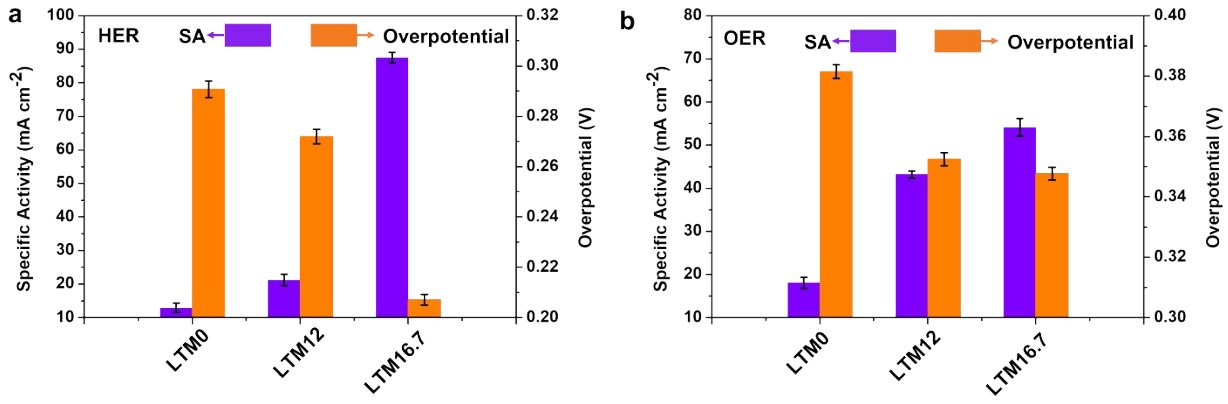

Fig. S7. (a) Overpotentials at 10 mA cm^{-2} and current density at -0.3 V vs RHE for HER; (b) Overpotentials at 10 mA cm^{-2} and current density at 1.6 V vs RHE for OER of LTM0, LTM12, and LTM16.7.

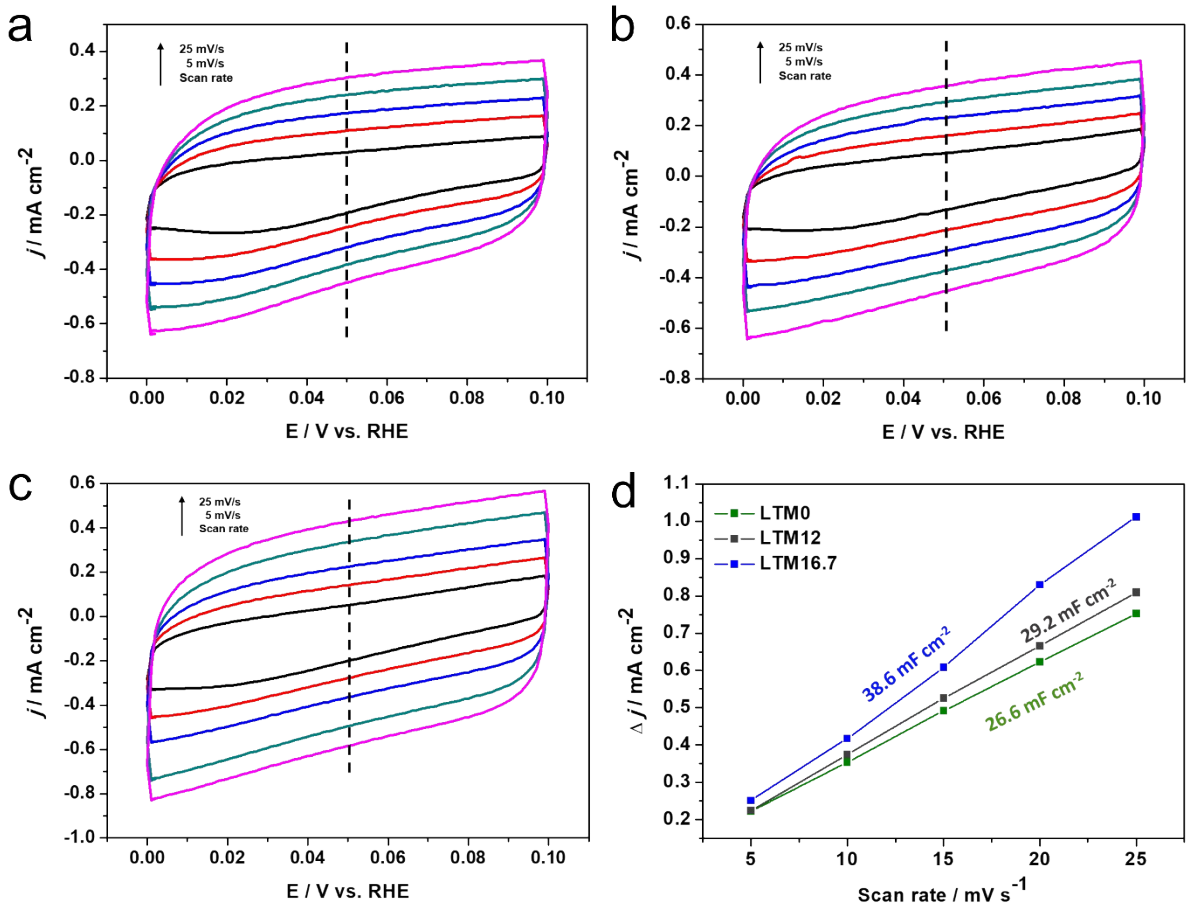

Fig. S8. The electric double layer capacitance measurements of (a) LTM0; (b) LTM12; (c) LTM16.7; and (d) the corresponding C_{dl} calculations, suggesting the variations of electrochemical surface area.

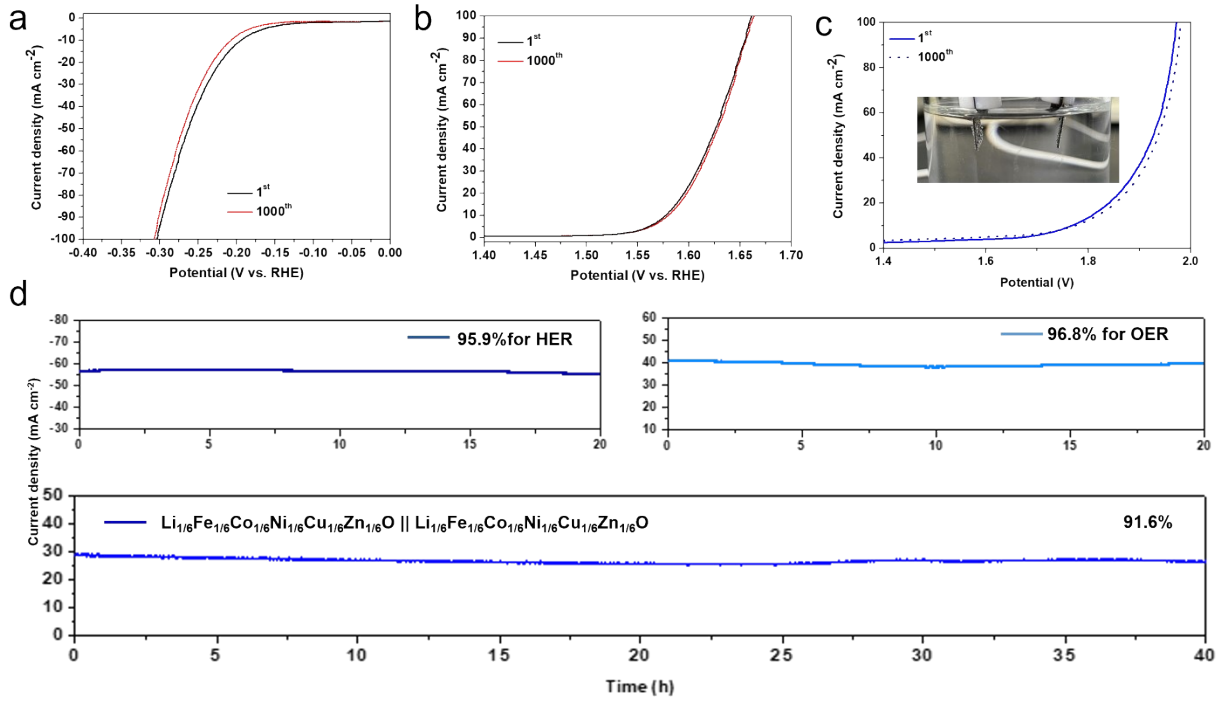

Fig. S9. 1st and 1000th polarization curves of LTM16.7 for (a) HER; (b) OER and (c) 2-electrode system, inset is the digital photo of 2-electrode system for overall water splitting; (d) Chronoamperometric measurement of LTM16.7 at a constant voltage for HER, OER and 2-electrode system.

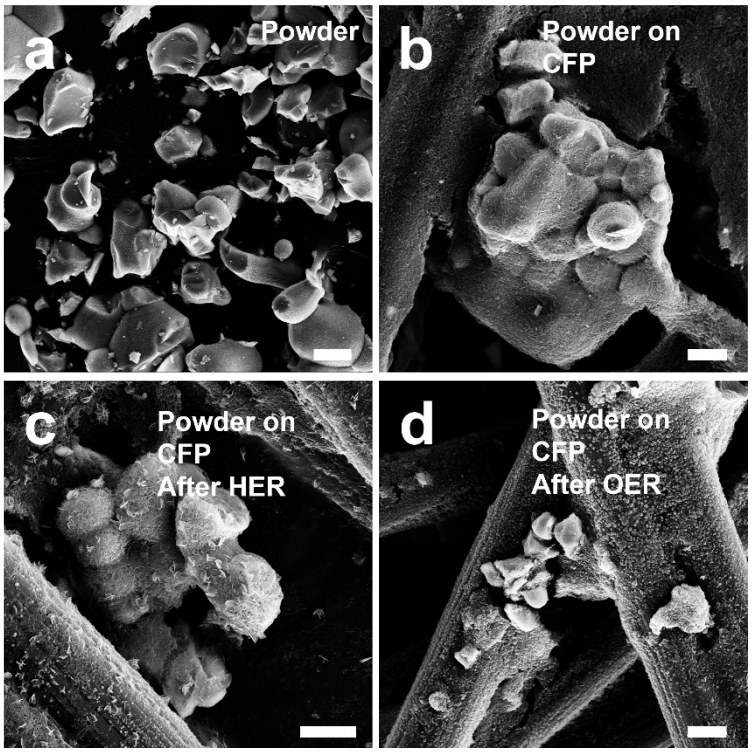

Fig. S10. SEM image of as-prepared LTM16.7: (a) Original powder; (b) Catalysts on the CFP; (c) After HER stability tests; (d) After OER stability tests.

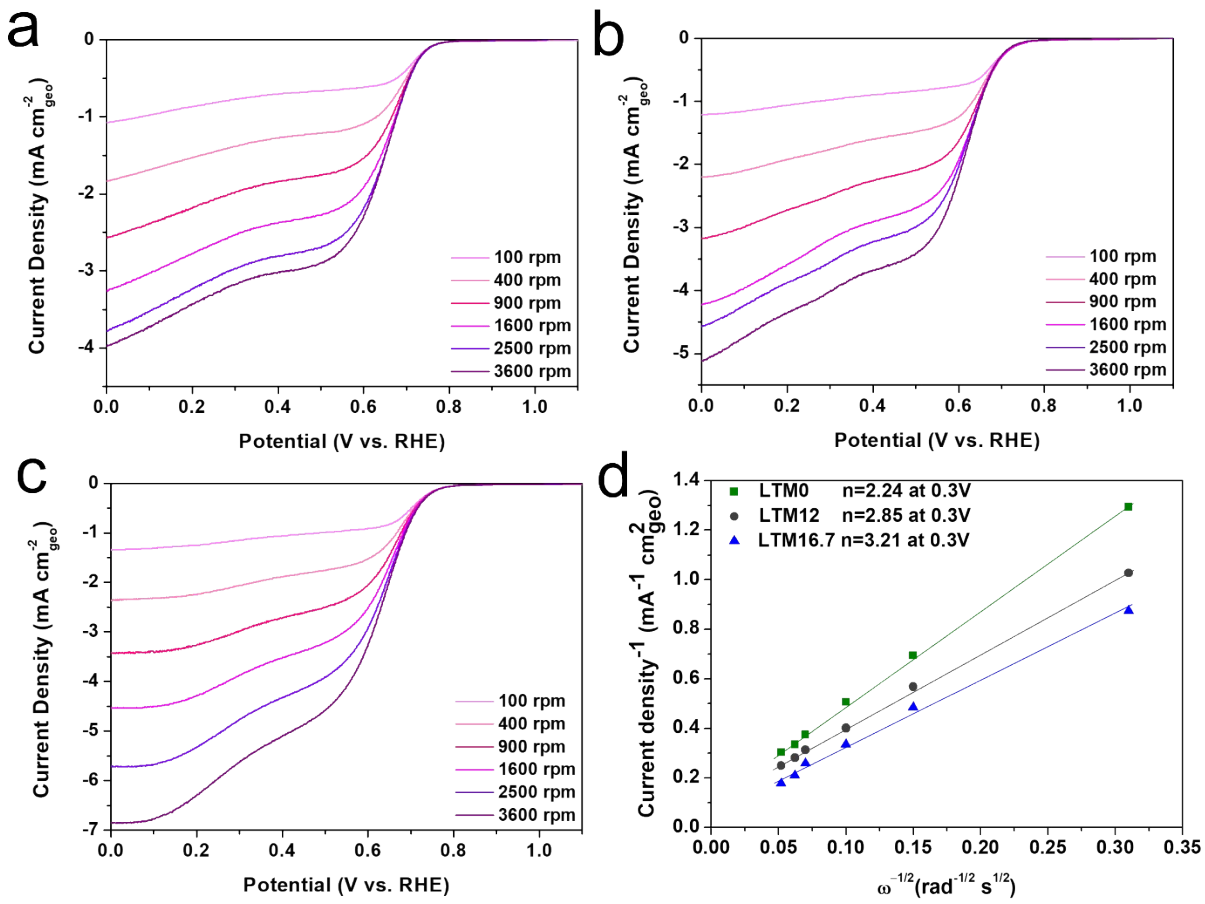

Fig. S11. LSV curves for the ORR on the RDE for (a) LTM0; (b) LTM12; and (c) LTM16.7 in O_2-saturated 0.1M KOH solution (scan rate: 5 mV s^{-1}) under different rotation speeds. (d) K-L plots at 0.3Vvs RHE for LTM series catalysts on the bases of the RDE data.

Koutecky-Levich (K-L) plots (j^{-1} vs $\omega^{-1/2}$) were analyzed to calculate the number of electrons (n) transferred based on K-L equation:

$$\frac{1}{j}=\frac{1}{j_L}+\frac{1}{j_k}=\frac{1}{B\omega^{1/2}}+\frac{1}{j_k}$$

$$B = 0.62nFC_o(D_o)^{2/3}\upsilon^{-1/6}$$

Where j_k is the kinetic current density, j is the measured current density, j_l is the diffusion-limiting current density, ω is the angular frequency of rotation (rad s^{-1}), F is the Faraday constant (96485 C mol^{-1}), C_0 is the bulk concentration of O_2 (1.21×10^{-6} mol cm^{-3}), D_0 is the diffusion coefficient of in 0.1 M KOH electrolyte (1.85×10^{-5} cm^2 s^{-1}), and v is the kinematic viscosity of the electrolyte (0.89×10^{-2} cm^2 s^{-1}). In K-L plots, the slope is $1/B$.[1]

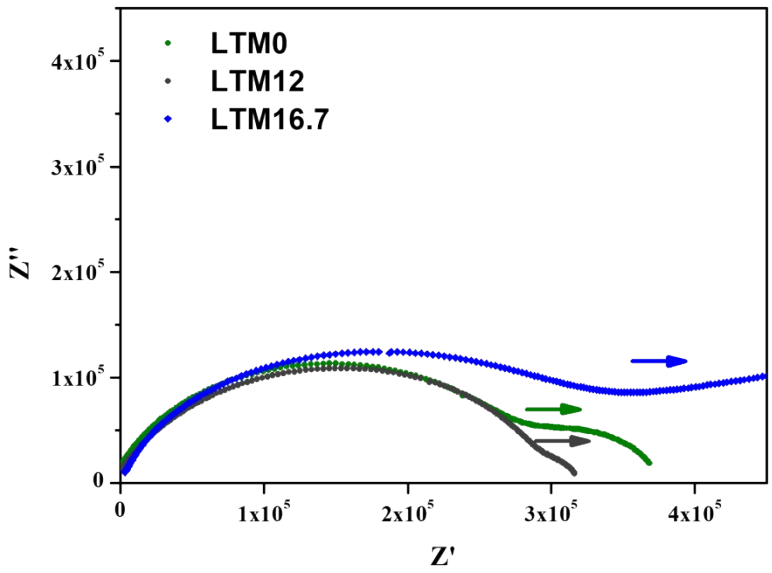

Fig. S12. Nyquist plots of LTM series catalysts with ceramic pellets under different temperature (LTM0:80℃; LTM12:80℃; LTM16.7: 25℃). The arrow marked with corresponded color represents that bulk area dominates charge transfer process under high frequency while grain boundary is the main carrier under low frequency.

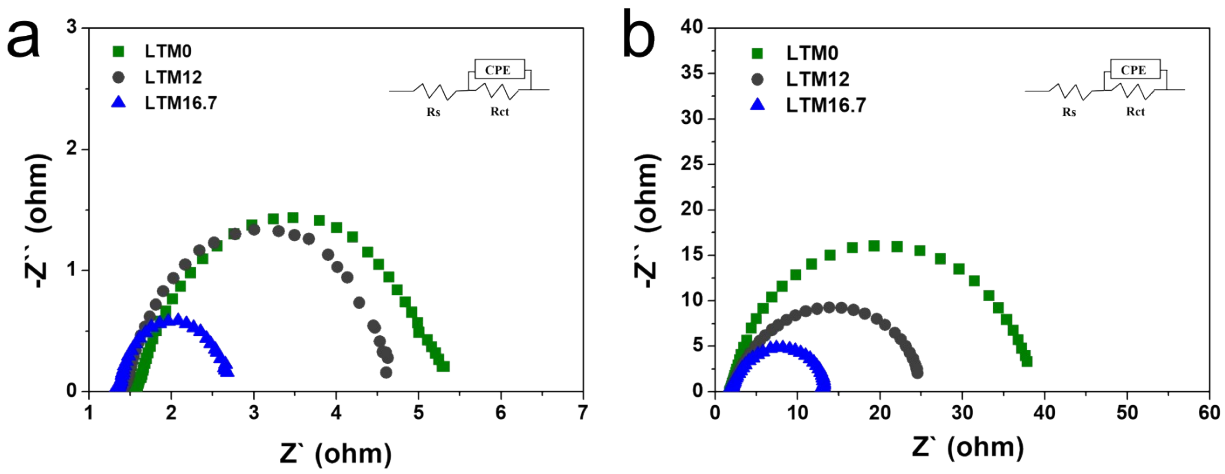

Fig. S13. Nyquist plots of the LTM series catalysts under (a) -0.3 V vs RHE and (b) 1.52 V vs RHE. The inset is the equivalent circuit.

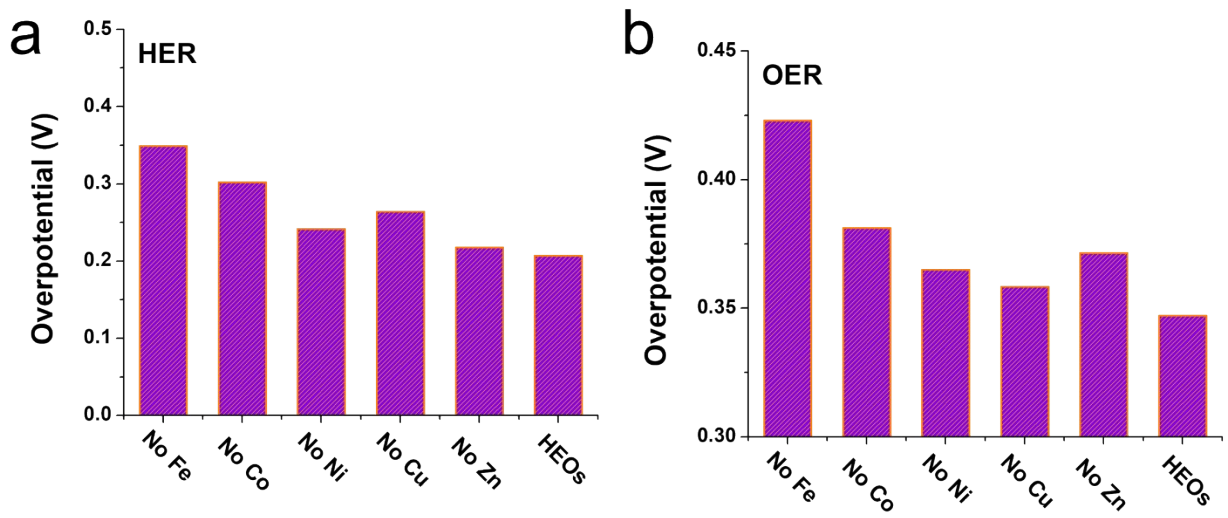

Fig. S14. Overpotentials at 10 mA cm^{-2} of composition alternation catalysts for (a) HER and (b) OER test.

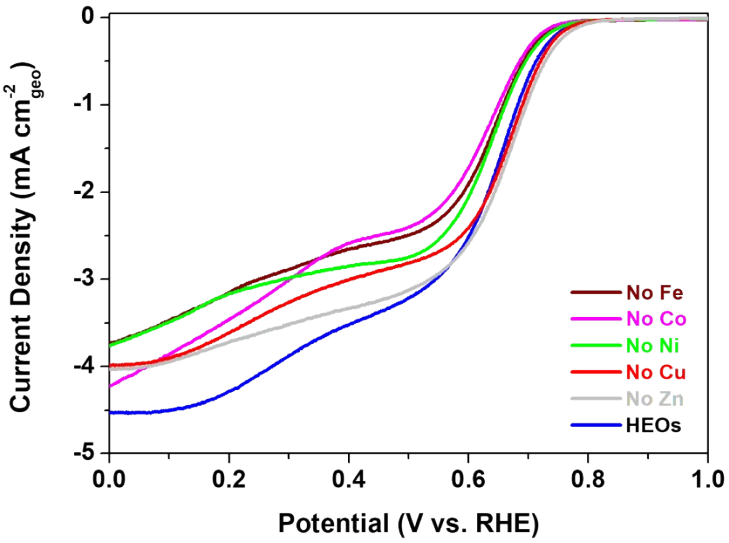

Fig. S15. LSV curves for the ORR on the RDE for composition alternation catalysts in O_2-saturated 0.1M KOH solution (scan rate: 5 mV s^{-1}) under 1600 rpm.

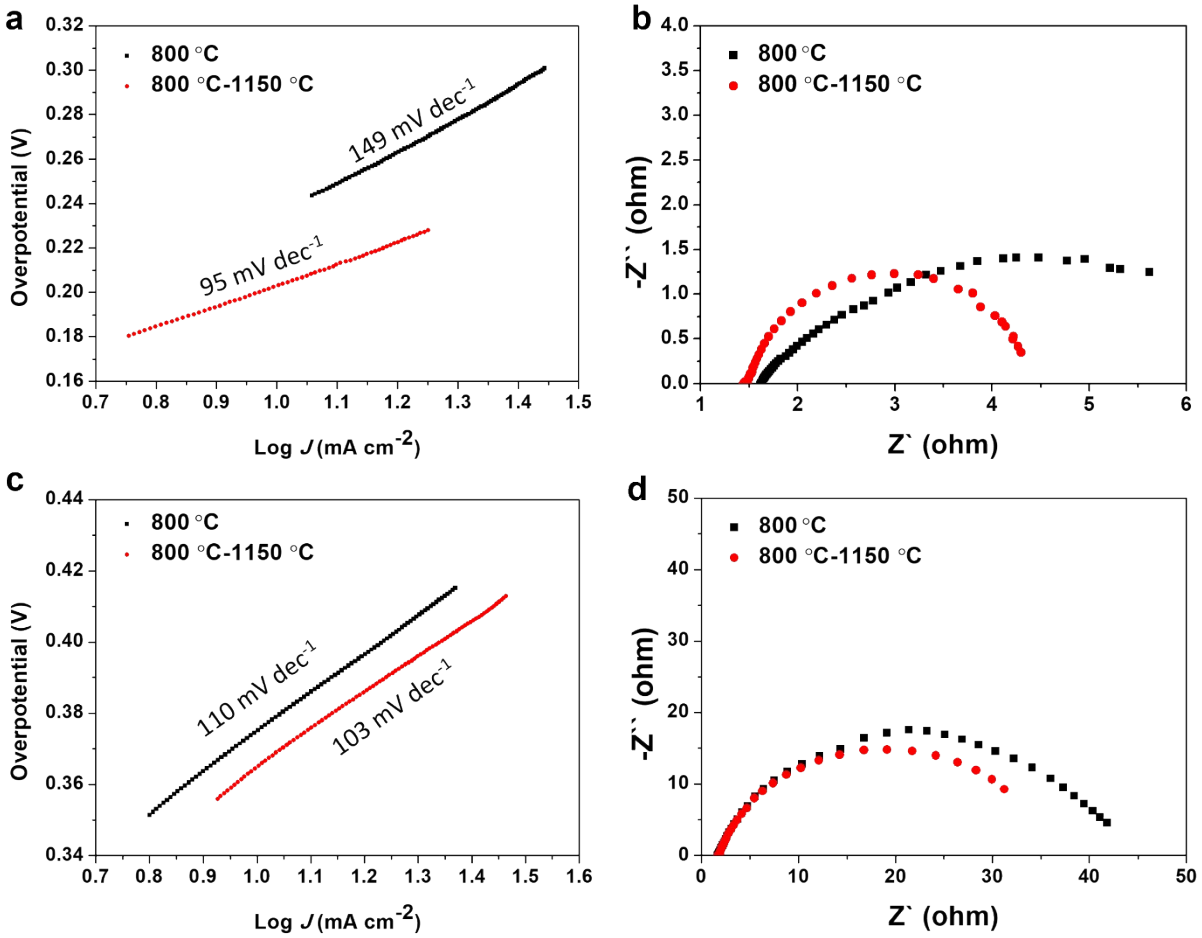

Fig. S16. Electrochemical performance of entropy reversibility: LTM16.7 sintered under 800℃ and back to 1150℃ again. (a) HER Tafel plots; (b) EIS under -0.3 V vs RHE; (c) OER Tafel plots; (d) EIS under 1.52 V vs RHE.

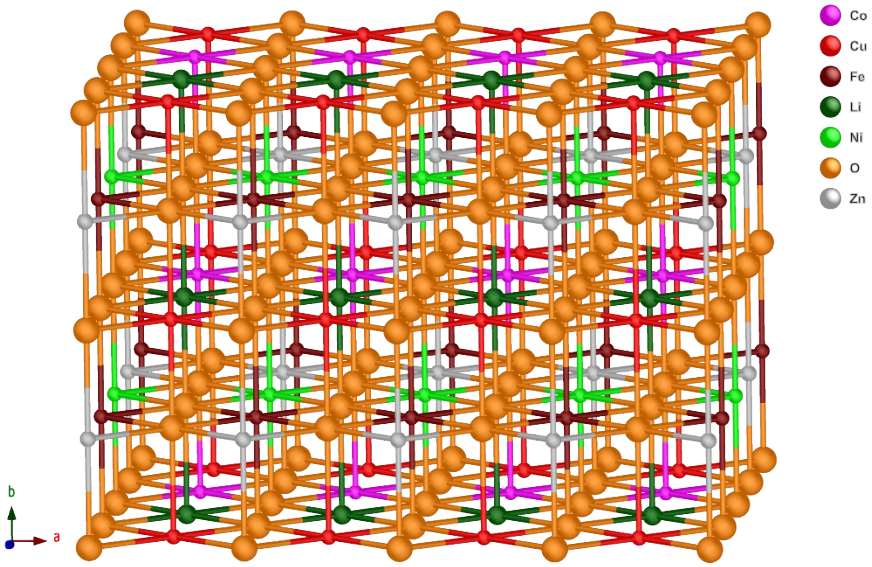

Fig. S17. The optimized structure of LTM16.7 model for the purpose of computation.

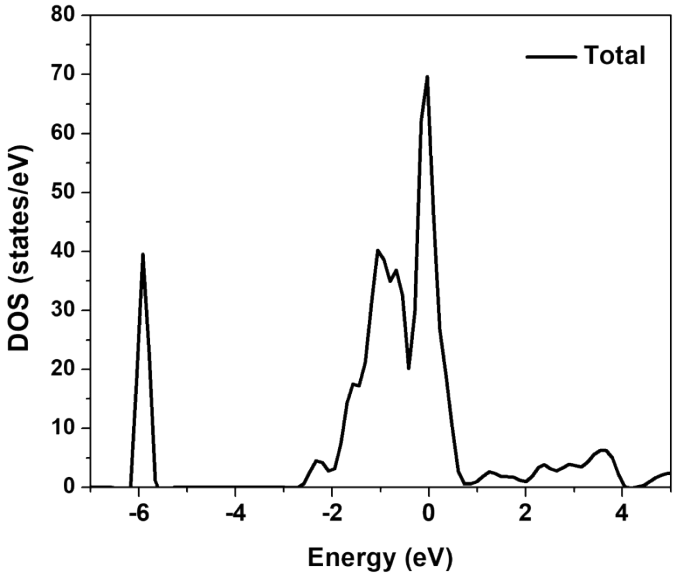

Fig. S18. Total density of state (DOS) of optimized model for LTM16.7.

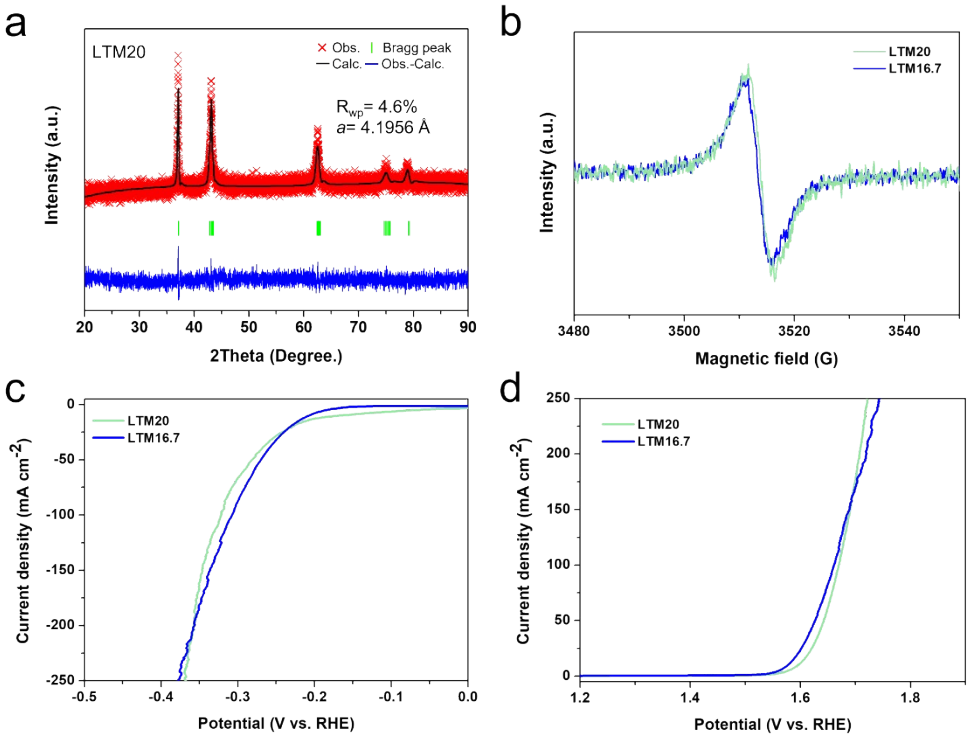

Fig. S19. (a) Powder XRD patterns and corresponding Rietveld refinement results of LTM20; (b) EPR spectra, (c) HER polarization curve, and (d) OER polarization curve of LTM16.7 and LTM20.

According to XRD pattern in Fig. S19a, the Rietveld refinement result yields the lattice constant *a* of 4.1946 Å for LTM20, which is almost unchanged in comparison with LTM16.7. And the EPR spectra also demonstrates that the intensity of LTM20 is slightly increased compared with LTM16.7, corresponds well with our conclusion for the relationship between lattice parameter and concentrations of oxygen vacancies. The most interesting result is that the HER and OER performance between LTM20 and LTM16.7 keeps almost unchanged.

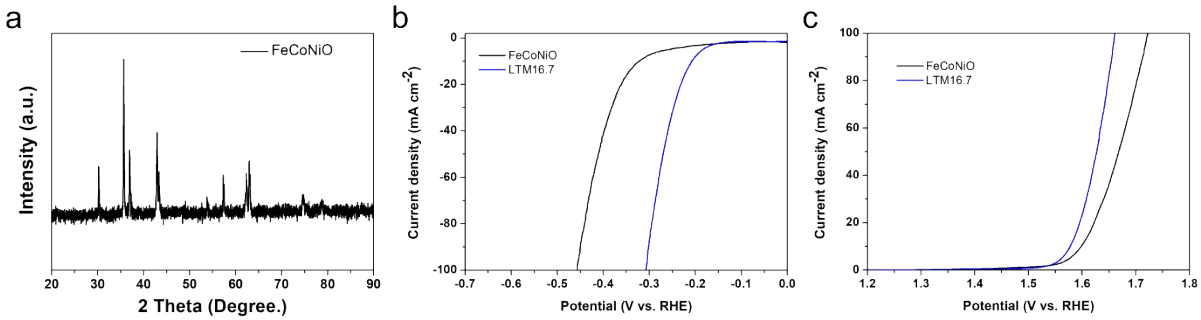

Fig. S20. (a) XRD pattern of as-prepared FeCoNiO; (b) HER and (c) OER polarization curves of FeCoNiO compared with LTM16.7.

The XRD pattern is shown in Fig. S20a, it can be seen that it is difficult to form one single phase for the low entropy oxides. In addition, the corresponding HER and OER activity of FeCoNiO cannot perform as well as LTM16.7 (Fig. S20b and c), indicating the importance of entropy stabilization.

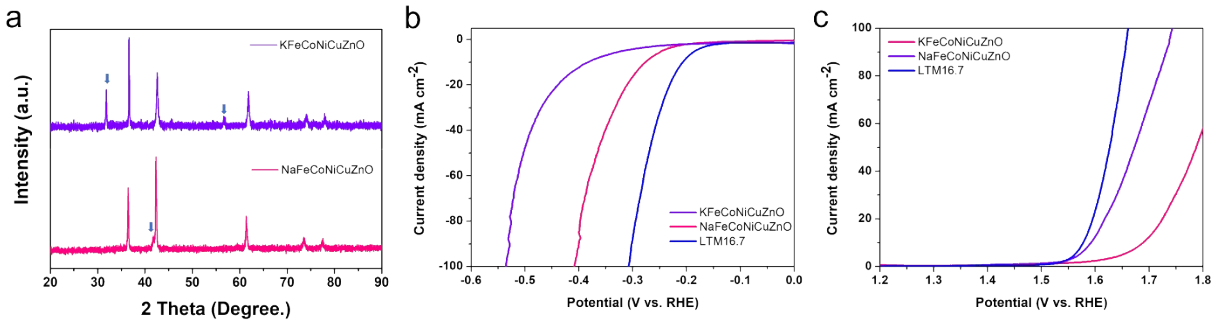

Fig. S21. (a) XRD pattern of KFeCoNiCuZnO and NaFeCuNiCuZnO, the blue arrows indicates the second phase, (b) HER and (c) OER polarization curves of KFeCoNiCuZnO and NaFeCuNiCuZnO compared with LTM16.7.

The XRD pattern of KFeCoNiCuZnO and NaFeCuNiCuZnO is shown in Fig. S21a, it can be seen that it is difficult to form one single phase for the larger ionic radius. In addition, the corresponding HER and OER activity of KFeCoNiCuZnO and NaFeCuNiCuZnO degrades apparently compared with LTM16.7 (Fig. S21b and c). As a result, Li was the only choice for mamipulating the LTM series samples.

Table S2. Summary of various electrocatalysts for HER

Electrocatalyst	Electrolyte	Overpotential @ 10 mA/cm^2 (mV)	Tafel slop (mV/dec)	Reference
PtFeNiLaCo-HEMG	0.1 M KOH	536	149	2
NiCoFeMnCrP	1 M KOH	220	94.5	3
CoP@BCN-1	1 M KOH	215	52	4
Fe_3C-Co/NC	1 M KOH	238	108.8	5
Co_2P	1 M KOH	247	64	6
NiFeOF	1 M NaOH	253	96	7
Co/CoP	1 M KOH	253	73.8	8
$Fe_5Ni_4S_8$	1 M KOH	236	61.8	9
NiFe LDH-NS@DG	1 M KOH	300	110	10
LTM16.7	1 M KOH	207	79.4	This work

Table S3. Summary of various electrocatalysts for OER

Electrocatalyst	Electrolyte	Overpotential @ 10 mA/cm^2 (mV)	Tafel slop (mV/dec)	Reference
$La_{0.5}Sr_{1.5}Ni_{1-x}Fe_xO_{4\pm\delta}$	0.1 M KOH	360	55	11
$La_{0.6}Ca_{0.4}Fe_{0.7}Ni_{0.3}O_{2.9}$	1 M NaOH	380	52	12
$La_{0.95}FeO_{3-\delta}$	0.1 M KOH	~410	48	13
$LaFe_xNi_{1-x}O_3$	1 M KOH	~350	64	14
$LaNi_{0.5}Fe_{0.5}O_3$	1 M KOH	340	59.6	15
$BaTiO_{3-\delta}$	0.1 M NaOH	>570	-	16
PtFeNiLaCo-HEMG	0.1 M KOH	377	150	2
CoCuFeMnNi-HEO	1 M KOH	400	76.7	17
MnFeCoNi-HEA	1 M KOH	377	99.6	18
CrMnFeCoNi-HEO	1 M KOH	354	66.3	19
LTM16.7	1 M KOH	347	53.8	This work

Reference

1. E. Jung, H. Shin, B. H. Lee, V. Efremov, S. Lee, H. S. Lee, J. Kim, W. Hooch Antink, S. Park, K. S. Lee, S. P. Cho, J. S. Yoo, Y. E. Sung and T. Hyeon, *Nat. Mater.*, 2020, **19**, 436-442.
2. M. W. Glasscott, A. D. Pendergast, S. Goines, A. R. Bishop, A. T. Hoang, C. Renault and J. E. Dick, *Nat. Commun.*, 2019, **10**, 2650.
3. D. Lai, Q. Kang, F. Gao and Q. Lu, *J. Mater. Chem. A*, 2021, **9**, 17913-17922.
4. H. Tabassum, W. Guo, W. Meng, A. Mahmood, R. Zhao, Q. Wang and R. Zou, *Adv. Energy Mater.*, 2017, **7**, 1601671.
5. C. C. Yang, S. F. Zai, Y. T. Zhou, L. Du and Q. Jiang, *Adv. Funct. Mater.*, 2019, DOI: 10.1002/adfm.201901949, 1901949.
6. K. Xu, H. Ding, M. Zhang, M. Chen, Z. Hao, L. Zhang, C. Wu and Y. Xie, *Adv. Mater.*, 2017, **29**, 1606980.
7. K. Liang, L. Guo, K. Marcus, S. Zhang, Z. Yang, D. E. Perea, L. Zhou, Y. Du and Y. Yang, *ACS Catal.*, 2017, **7**, 8406-8412.
8. Z.-H. Xue, H. Su, Q.-Y. Yu, B. Zhang, H.-H. Wang, X.-H. Li and J.-S. Chen, *Adv. Energy Mater.*, 2017, **7**, 1602355.
9. Y. Wu, F. Li, W. Chen, Q. Xiang, Y. Ma, H. Zhu, P. Tao, C. Song, W. Shang, T. Deng and J. Wu, *Adv. Mater.*, 2018, **30**, 1803151.
10. Y. Jia, L. Zhang, G. Gao, H. Chen, B. Wang, J. Zhou, M. T. Soo, M. Hong, X. Yan, G. Qian, J. Zou, A. Du and X. Yao, *Adv. Mater.*, 2017, **29**, 1700017.
11. R. P. Forslund, W. G. Hardin, X. Rong, A. M. Abakumov, D. Filimonov, C. T. Alexander, J. T. Mefford, H. Iyer, A. M. Kolpak, K. P. Johnston and K. J. Stevenson, *Nat. Commun.*, 2018, **9**, 3150.
12. S. V. Porokhin, V. A. Nikitina, D. A. Aksyonov, D. S. Filimonov, E. M. Pazhetnov, I. V. Mikheev and A. M. Abakumov, *ACS Catal.*, 2021, **11**, 8338-8348.
13. Y. Zhu, W. Zhou, J. Yu, Y. Chen, M. Liu and Z. Shao, *Chem. Mater.*, 2016, **28**, 1691-1697.
14. H. Wang, J. Wang, Y. Pi, Q. Shao, Y. Tan and X. Huang, *Angew. Chem. Int. Ed.*, 2019, **58**, 2316-2320.
15. Q. Guo, X. Li, H. Wei, Y. Liu, L. Li, X. Yang, X. Zhang, H. Liu and Z. Lu, *Front. Chem.*, 2019, **7**, 224.
16. C.-F. Chen, G. King, R. M. Dickerson, P. A. Papin, S. Gupta, W. R. Kellogg and G. Wu, *Nano Energy*, 2015, **13**, 423-432.
17. D. Wang, Z. Liu, S. Du, Y. Zhang, H. Li, Z. Xiao, W. Chen, R. Chen, Y. Wang, Y. Zou and S. Wang, *J. Mater. Chem. A*, 2019, **7**, 24211-24216.
18. W. Dai, T. Lu and Y. Pan, *J. Power Sources*, 2019, **430**, 104-111.
19. T. X. Nguyen, Y. C. Liao, C. C. Lin, Y. H. Su and J. M. Ting, *Adv. Funct. Mater.*, 2021, **31**, 2101632.